Atmospheric Research 336 (2026) 108865

Contents lists available at ScienceDirect

Atmospheric Research

journal homepage: www.elsevier.com/locate/atmosres

On the accuracy of optical disdrometer measurements

Enrico Chinchella [a,b], Arianna Cauteruccio [a,b], Luca G. Lanza [a,b,*]

[a] Department of Civil, Chemical and Environmental Engineering, University of Genova, Genoa 16145, Italy
[b] WMO Measurement Lead Centre "B. Castelli" on Precipitation Intensity, Genoa 16145, Italy

ARTICLE INFO

Dataset link: Supplementary to "On the accuracy of optical disdrometer measurements" (Original data)

Keywords:
Rainfall
Disdrometer
Measurement accuracy
Raindrop generator
Drop size distribution
Fall velocity

ABSTRACT

Disdrometers are widely used to measure the microphysical properties of precipitation, synthesised by the drop size and fall velocity distribution, and to infer integral properties like rainfall intensity, kinetic energy, visibility and radar reflectivity. Although often used to validate other methods of inferring precipitation products, including radar, satellite and opportunistic sensors, the accuracy and reliability of disdrometer measurements are rarely quantified. This study is the first to traceably and systematically quantify the instrumental bias of optical disdrometer measurements in the laboratory. We tested two widely used optical transmission disdrometers, the OTT Parsivel^2 and the Thies LPM, using a raindrop generator that was specifically developed for calibrating non-catching precipitation measurement instruments. We also conducted tests using metallic spheres and demonstrated that the calibration obtained using artificial particles is not appropriate for optical disdrometers. The instruments investigated significantly underestimate drop size by up to 20%, with peaks of up to 40% for the Thies LPM when using the internal post-processing algorithm. The OTT Parsivel^2 overestimates fall velocity by about 5 to 10%, while the Thies LPM underestimates it by up to 15%. Slight linear trends of the percentage relative bias with drop size are observed for both drop diameter and fall velocity. However, adjustment of field measurements may be challenging, given the large dispersion observed. The mean bias and dispersion of drop size and velocity measurements vary along and across the laser beam, especially for the Thies LPM, with differences of up to 30% observed between drops falling at the opposite edges of the beam. Integral properties are largely underestimated, particularly at low rainfall intensity, although performance improves as intensity increases. These results highlight the importance of laboratory calibration to assess and quantify the instrumental bias of disdrometer measurements prior to their use in research or operational applications, especially when used to calibrate meteorological radars or to compare integral measurements with those of other instruments that measure precipitation in situ. While they provide relevant information about individual drop size and velocity, optical disdrometers need to be further improved before they can compete reliably with traditional rain gauges in measuring rainfall intensity.

1. Introduction

Atmospheric (liquid and solid) precipitation is increasingly being measured using non-catching gauges (NCGs). These instruments have no moving parts, collector or storage tank, thus reducing the cost of ordinary maintenance typically associated with catching-type gauges (Lanza et al., 2021). NCGs are generally distrometers, more commonly named 'disdrometers', as they measure the frequency distribution of the size and fall velocity of hydrometeors passing through or impacting their sensing area. This is expressed as the Particle Size and Velocity Distribution (PSVD), either at a given temporal resolution (e.g., one minute) or integrated at the event scale. Useful derived variables can then be obtained, including precipitation type, precipitation intensity or amount, kinetic energy, visibility and radar reflectivity.

Disdrometers can use optical, acoustic (vibration) or microwave (radar) measurement principles. Optical disdrometers can take non-contact measurements because they have a transmitter that emits visible or infrared light and an optical sensor that receives the signal. Depending on the type and configuration of their receiver, they can be classified as optical transmission, forward scattering, backward scattering, or imaging sensors (Kathiravelu et al., 2016). In the case of optical transmission sensors, the presence of hydrometeors in the instrument's sensing area (obstruction) reduces the received signal. This signal is then processed to derive the hydrometeors' geometric (size) and

* Corresponding author at: Department of Civil, Chemical and Environmental Engineering, University of Genova, Genoa 16145, Italy.
E-mail address: luca.lanza@unige.it (L.G. Lanza).

https://doi.org/10.1016/j.atmosres.2026.108865
Received 28 October 2025; Received in revised form 12 February 2026; Accepted 13 February 2026
Available online 14 February 2026

dynamic (velocity) characteristics. Light scattering instruments measure the signal reflected by hydrometeors crossing their sensing volume, while imaging sensors photograph single or multiple hydrometeors in the visible or infrared spectrum. Impact disdrometers, on the other hand, measure the kinetic energy of hydrometeors that hit on a membrane or plate. The vibrations or deformation generated by the impact are converted into an electrical signal. The frequency spectrum of this signal can be used to determine the number and size of the drops, provided that a relationship between drop size and fall velocity is assumed (Tuukka, 2015). Microwave or radar disdrometers operate in a similar manner to traditional meteorological radars, except they lack horizontal scanning capabilities and sample a narrow vertical cone above the instrument (see e.g. Sheppard, 1990).

Since their initial appearance (see Joss and Waldvogel, 1967), disdrometers have been widely used as a ground reference for developing or validating precipitation retrieval algorithms for weather radars, satellite borne and opportunistic sensors. In the case of radar measurements, they were initially used to establish the relationship between radar reflectivity (Z) and rainfall rate (RI). More recently, they have also been used to validate algorithms for retrieving the Drop Size Distribution (DSD) from Doppler radar measurements (see e.g., Schleiss and Smith, 2015; Gorgucci et al., 2001; Bringi et al., 2003; Anagnostou et al., 2008; Conrick et al., 2020; Gatidis et al., 2022). Disdrometers are also involved in the validation of satellite precipitation measurements (see e.g., Peinó et al., 2024) as the Core Satellite product of the Global Precipitation Measurements (GPM) initiative (Wu et al., 2019; Petersen et al., 2020; Tokay et al., 2020; Adirosi et al., 2021) and in the calibration of the Tropical Rainfall Measuring Mission (TRMM) (Kummerow et al., 2000), both NASA's projects. An optical disdrometer was specifically designed for in situ shipboard measurements in the Ocean Rainfall And Ice-phase precipitation measurements Network (Ocean RAIN) from June 2010 to April 2017. The precipitation parameters obtained were used for validation of satellite data, as the GPM and the Hamburg Ocean Atmosphere Parameters and fluxes from Satellite (HOAPS) data (Burdanowitz et al., 2018), and the study of retrievals (Aragon et al., 2024). The factory calibration of the disdrometers is used in the various studies, with no verification carried out (Kummerow et al., 2000), and in some cases, evident biases remain in the DSD's assessment (Tapiador et al., 2017).

Disdrometer measurements are also used as a reference for both the precipitation intensity and the DSD when validating newly developed measurement methods, like e.g. opportunistic sensors. These sensors exploit already existing but usually unrelated measurements (mostly from communication technologies) to infer the precipitation amount or intensity by interpreting the undesired effect induced by raindrops on the received signal (Giannetti and Lanza, 2023). For example, changes of the signal intensity in telecommunication microwave links (Fencl et al., 2020; Špačková et al., 2021), in images obtained from surveillance cameras (Lee et al., 2023) or in satellite to earth communications (Colli et al., 2019).

The possibility to infer the kinetic energy of raindrops from disdrometer measurements is exploited in soil erosion studies, for instance to obtain erosivity-intensity relationships (see e.g. Nanko et al., 2016). They are also used as a reference when developing rainfall generators in field or laboratory experiments (see e.g., Jadhao et al., 2023; Gires et al., 2020). Disdrometers also provide valuable datasets for validating climatic and meteorological models that require in-depth knowledge of precipitation microphysical properties (see e.g. Tapiador et al., 2018; Yang et al., 2019). The measurement of the DSD has significant implications for other research fields that are becoming increasingly relevant. For example, it is used to study leading-edge erosion in wind turbines (Pryor et al., 2022), to investigate possible correlations with fulmination in convective precipitation events (Chatterjee and Das, 2020) and to assess the impact of throughfall in forest canopies (Levia et al., 2017). In terms of technical applications, disdrometers are also being increasingly adopted in the transportation sector. They are used to monitor visibility and detect snowfall and other hazardous environmental conditions near roads, airports and other key infrastructure (Mocholí Belenguer et al., 2020).

Despite their widespread use, it is rare for the accuracy and reliability of disdrometer measurements to be questioned or quantified, and end users are rarely aware of their potential biases. They are often considered the 'ground truth', based on factory calibration provided by the manufacturer. However, several studies show that significant inconsistencies are present in disdrometer measurements. Results also tend to be instrument-dependent, indicating the presence of some instrumental bias that may affect research outcomes (Adirosi et al., 2018; Johannsen et al., 2020a; Campos and Zawadzki, 2000). This is evident from field intercomparison results, where significant discrepancies in measurements are evident (see, for example, Lanza and Vuerich, 2009; de Moraes Frasson et al., 2011; Park et al., 2017). A few authors also report evidence of significant bias in the drop fall velocity measurements obtained from disdrometers (see, e.g., Beczek et al., 2025, Saha and Testik, 2023). Tokay et al. (2001) conducted a comparison of three disdrometers (two optical and one impact) against each other and against the rain totals measured by tipping-bucket rain gauges in a field experiment. While the DSDs demonstrated good consistency between the two types of disdrometer, both underestimated the rain totals, likely due to the underreporting of small- to medium-sized drops.

Dedicated laboratory calibration is necessary to minimise the instrumental bias of disdrometer measurements, at least for liquid precipitation. However, while calibration is relatively straightforward for traditional catching-type precipitation gauges (as they measure continuous water flow, which can be easily reproduced using precision pumps — see Colli et al., 2014), disdrometers measure individual raindrops. Therefore, to provide a calibration reference quantity, drops of known diameter and fall velocity must be produced individually. The technical challenges include the wide range of drop diameters required to reproduce the DSD of natural rainfall, and the need for an independent measurement of drop characteristics immediately prior to them crossing or impacting the sensing area/volume of the instrument under test. There is no agreed calibration procedure in the literature. Manufacturers often do not disclose their calibration procedure or only provide limited information. In some cases, instruments are tested using only large diameter drops (larger than 2 mm), or drops are replaced with metallic spheres or glass beads. A traceable reference may be absent for the drops, or it may be obtained using the same measuring principles as the instrument under test. Lanza et al. (2021) provided a review of current calibration procedures applied by manufacturers and researchers to assess the accuracy of disdrometer measurements.

The calibration procedure is disclosed for instance by Distromet Ltd., the manufacturer of the Joss-Waldvogel RD-80 impact disdrometer, which is used to measure the size distribution of raindrops. The sensor converts the mechanical momentum of an impacting drop into an electric pulse whose amplitude is approximately proportional to the mechanical momentum (Disdromet, 2022). Calibration is performed using real drops with a diameter of approximately 0.8 mm, falling at near terminal velocity. These drops are evenly distributed over the entire sensing area. Adjustments are then made and the drop test is repeated. However, full calibration over the entire range of natural raindrop diameters is not performed. Lane et al. (2014) proposed in situ calibration as a strategy towards implementation and deployment of low-cost disdrometers by describing a calibration algorithm using laser scattering as a DSD second moment observable to supplement rain gauge based rain rate DSD moment observables. Although the study was conducted using an impact disdrometer, the authors claim that the proposed procedure can be applied to optical and other types of disdrometers.

A metrologically sound procedure for the laboratory calibration of disdrometers was developed during the European project 'INCIPIT: Calibration and accuracy of non-catching instruments to measure liquid/solid atmospheric precipitation', which was financed in 2019 by EURAMET (the European Association of Metrology Institutes) under

EMPIR, the European Metrology Programme for Innovation and Research (Merlone et al., 2022). The calibration procedure is currently being evaluated as a potential European Standard by Technical Committee TC318 (Hydrometry) of CEN, the European Committee for Standardization. Three different rain drop generators suitable for calibrating NCGs were developed during the project, and their characterisation was performed to derive their calibration uncertainty (Baire et al., 2022).

The present study presents and discusses the results of an extensive laboratory calibration performed using an existing rain drop generator developed at the University of Genoa during the INCIPIT project. The calibration, following the above-mentioned procedure, was performed on two widely used optical disdrometers. The aim was to derive information about their measurement accuracy and the potential biases associated with measuring drop size and fall velocity, and the derived integral properties of precipitation. The organisation of the paper is as follows: Section 2 provides basic information about the characteristics of the two optical disdrometers under test and describes the rain drop generator and the adopted calibration procedure. Section 3 investigates the effect that drop shape may produce on calibration results and quantifies the instrumental bias in the measurement of drop size and fall velocity. The propagation of such bias to derived variables, such as rainfall intensity, kinetic energy and radar reflectivity is also quantified. Finally, conclusions are drawn in Section 4.

2. Material and methods

2.1. Optical disdrometers under test

We tested two widely used optical transmission disdrometers: the Parsivel^2 present weather sensor manufactured by OTT HydroMet GmbH (OTT Hydromet GmbH, 2017) and the Laser Precipitation Monitor (LPM), manufactured by Thies CLIMA, Adolf Thies GmbH & Co. KG (Thies A., 2011). Both instruments are equipped with a laser emitter and a receiving sensor, that are horizontally aligned and connected to the instrument main body by means of supporting arms. A laser diode is used for producing a thin light beam, 30 mm wide for the OTT Parsivel^2 and 20 mm wide for the Thies LPM. Interference from ambient light is minimized by operating the laser diode of the Thies LPM at high frequency (173 kHz) and using a low-pass filter in the receiver, while the operating frequency of the OTT Parsivel^2 is not provided in the operating instructions (OTT Hydromet GmbH, 2017).

In both instruments, the power of the laser beam is converted into an electrical signal by a photodiode in the receiver head and is reduced by the light blockage due to hydrometeors crossing the beam. The power drop is proportional to the size of the falling hydrometeor while the fall velocity is obtained from the duration of the beam blockage (extinction). The combination of hydrometeor size and fall velocity, together with the measurement of local temperature, makes it possible to identify the type of precipitation (e.g. drizzle, rain, snow, soft hail, hail and mixed) and to exclude objects other than hydrometeors that may cross the laser beam, such as insects, since the size-velocity relationship would not be consistent with that expected for hydrometeors (e.g. provided by Gunn and Kinzer, 1949).

For the OTT Parsivel^2, the diameter of liquid hydrometeors is reported in 32 classes, ranging from 0.2 to 8 mm (extended to 25 mm for solid hydrometeors), while the fall velocity is reported in 32 classes, spanning a range of 0.2 to 20 m/s. The precipitation type is categorized in 8 classes, from drizzle to hail. The diameter of liquid hydrometeors is instead reported in 22 classes for the Thies LPM, ranging from 0.125 to ≥8 mm, while the fall velocity is reported in 20 classes, spanning a range of 0.2 to ≥10 m/s. The precipitation type is categorized in 10 classes, from drizzle to hail. The hydrometeor size and fall velocity distribution over the class binning, aggregated at 1 min resolution, is also used to calculate the intensity and amount of precipitation, visibility, kinetic energy of precipitation and radar reflectivity.

Both instruments transmit a single data telegram at a fixed interval that can be configured by the user (usually set to one minute). The typical output telegram provides the PSVD matrix, but raw measurements can also be included in the form of a list of each hydrometeor detected, with its size (diameter) and fall velocity information. In our tests, the OTT Parsivel^2 was set as to report both the raw measurements and the PSVD matrix, although the latter information is affected by an undisclosed filtering software (Saha and Testik, 2023). In particular, the PSVD matrix was consistently empty for small drops (1 mm in diameter or lower) or if less than 10 to 15 larger drops were detected in one minute, and this prevented us to test results for the PSVD matrix of the OTT Parsivel^2. In the case of the Thies LPM, instead, two separate tests were performed to test the two telegrams since the instrument cannot output both values at the same time. It is also worth noting that – while ideal for testing the gauge – rarely output telegrams containing raw measurements are used in the field due to the large amount of data produced and the risk of overwhelming the communication protocol during intense precipitation events.

The operating instructions for the OTT Parsivel^2 (OTT Hydromet GmbH, 2017) state that the instrument reports the equivolumetric drop diameter, with no further information provided regarding the filtering and processing of raw data. Battaglia et al. (2010) reported an internal correction algorithm for an earlier version of the instrument which was not mentioned in the operating manual. Such information is not available for the current version of the instrument, and applying the effects of this correction to measurements would produce unrealistic results. Therefore, we have assumed that this correction is no longer implemented in the OTT Parsivel^2. For the Thies LPM, two different values of diameter and drop fall velocity are reported. The first is labelled "spheres", while the second is labelled "hamburger", with no further information provided on how this shape is obtained. To maintain consistency between the two instruments, the first value (spheres) was used, on the assumption that it refers to the equivolumetric diameter of the drop.

Measurement errors may arise in optical transmission sensors depending on where and when the drop crosses the laser beam. The disdrometer would report a drop size smaller than the actual size if the drop crossed the sensing area at the edge of the laser beam. The total water volume would be instead overestimated if two drops crossed the laser beam at the same time, as the entire blockage would be considered as a single larger drop. In the laboratory tests, however, drops were released one by one, ensuring that they fall entirely inside the instrument sensing area.

Environmental factors may also add to measurement bias. The manufacturer's installation instructions provide specific indications regarding the orientation of the disdrometer on site. According to the 'Instructions for Use' (Thies A., 2011), the laser beam of the Thies LPM should be oriented towards the south (±10°) in the northern hemisphere. The receiver head should be positioned on the south side to minimise the impact of sunlight on the sensor. Meanwhile, the 'Operating Instructions' of the OTT Parsivel^2 (OTT Hydromet GmbH, 2017) suggests that the laser beam should be perpendicular to the main wind direction. It is also noted that glare and intense sunlight may have an impact on the measurements. Though not addressed in this work, wind is undoubtedly the largest source of environmental bias under operating conditions (Lanza and Cauteruccio, 2022). The magnitude of the wind-induced bias on disdrometer measurements can be assessed using numerical simulation and at least partially corrected by means of adjustment curves as a function of the wind speed and direction (see e.g. Chinchella et al., 2024, 2025).

Nevertheless, the manufacturer declares that the error on the measurement of precipitation intensity (rain equivalent) from the Thies LPM (compared with an unspecified reference sensor, at wind speed <3 m/s) is ≤15% for rainfall (at intensity up to 20 mm/h), and ≤ 30% for snow (Thies A., 2011). The declared accuracy of rain rate measurements for the OTT Parsivel^2 is ±5%, while the accuracy degrades to ±20% in case

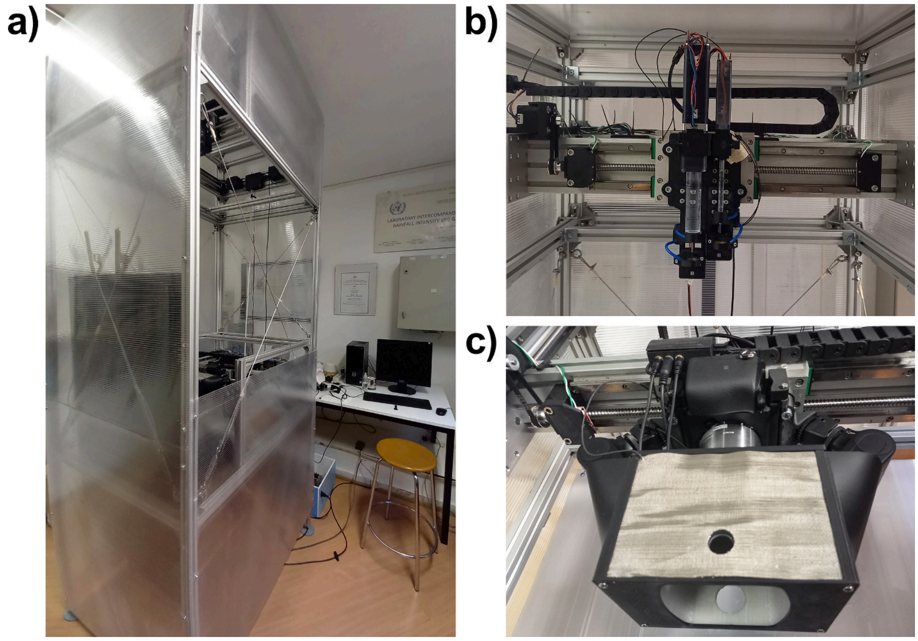

Fig. 1. a) The CRG installed in the Precipitation Measurement Laboratory of the University of Genova, Italy. b) Close-up view of the DRH, showing the syringe pumps and nozzles that are used to release water drops. c) Close-up view of the PVS with the camera and the macro lens attached, the light diffuser with two small apertures to allow drops to pass through and two speedlights positioned on either side.

of solid precipitation (OTT Hydromet GmbH, 2017).

2.2. The raindrop generator and calibration procedure

The laboratory tests were conducted using the Calibrated Rainfall Generator (CRG), shown in Fig. 1a, developed by the University of Genova as part of the above-mentioned INCIPIT project (Merlone et al., 2022). The device is situated within the Precipitation Measurement Laboratory of the University of Genova, which forms part of the Measurement Lead Centre "*B. Castelli*" of the World Meteorological Organisation (WMO).

The CRG uses a Drop Releasing Head (DRH) to produce and release water drops of varying diameters, ranging from 0.6 to 5.5 mm. Released drops are then independently measured – to establish their diameter and fall velocity – by a Photogrammetric Verification System (PVS). Precise alignment between the disdrometer sensing area, the DRH and the PVS is ensured by a motorised gantry. The entire system is enclosed within aluminium profiles and plastic panels forming a cage to protect falling drops from air gusts that could affect their trajectory.

The DRH was designed to generate and release – on demand – a single water drop of chosen diameter. This is achieved by means of two syringe pumps, assisted by an electrostatic release system. The two pumps were made using readily available plastic syringes and hollow-shaft stepper motors, relying mostly on 3D-printed parts for the remaining components. A threaded rod – passing through the motor shaft – is used to exert pressure on the syringe plunger, generating the water flow. A photo of the two pumps installed in the DRH is shown in Fig. 1b. The smaller pump has a capacity of 1 ml, with a movement resolution of 0.001 mm and a volume resolution of 0.023 μl. The larger pump has a capacity of 20 ml, and a movement and volume resolution of 0.0013 mm and 0.35 μl, respectively. The water volume displaced by the pump results in a drop that remains attached to the tip of the nozzle without falling. The drop is then released applying high voltage – generated by a 5 V to 5 kV DC-DC converter – between the nozzle and a metal ring positioned just below it. The negatively charged water drop is attracted to the positively charged metal ring due to the electrostatic force, resulting in the drop detachment. The electrostatic force experienced by the drop can be precisely tuned by controlling the ring position – adjusted in three dimensions using alignment screws – and by controlling the duration of the voltage application. Depending on the required drop diameter, different nozzle sizes may be employed.

For use as a traceable reference, the diameter and fall velocity of the drops produced by the DHR must be measured prior to their arrival at the sensing area of the instrument. To ensure no interference with the drop trajectory, a photogrammetric approach is used. The PVS employs a camera with a 24-megapixel APS-C CMOS sensor, in combination with a macro lens. The system – which is capable of a 1:1 reproduction ratio – provides a maximum spatial resolution of 3.89 μm. The PVS produces multiple images of a single drop using stroboscopic illumination provided by speedlights. When the camera shutter opens, three or more flashes of light are emitted at 2.5-millisecond intervals, thus "freezing" multiple images of the drop in flight. The camera shutter then closes producing a single picture. Precise synchronization between the PVS and the DHR ensures that the camera shutter opens just before the drop enters the camera's field of view. For improving accuracy and simplify images post-processing, a specially designed diffuser is employed in combination with two compact speedlights. This provides uniform illumination of the falling drop, highlighting its contour against a black background. An image of the PVS including the camera, the speedlights and the light diffuser is shown in Fig. 1c.

Depending on the drop size and the release height, the fall velocity of the drops upon reaching the disdrometer sensing area may approach their terminal velocity, defined as the maximum velocity attainable by an object as it falls through a fluid. This condition is reached when the total drag and buoyancy forces acting on an object counterbalance the force of gravity, meaning that the object is no longer accelerating (Lanza et al., 2021). However, due to space constrains, a maximum release height of 1.2 m was possible in the laboratory tests, and larger drops could not reach their terminal velocity. A detailed characterisation of the CRG, including an assessment of the associated calibration uncertainty and performances, can be found in the work of Baire et al. (2022).

The use of metallic spheres is a relatively common approach for testing the performance of optical disdrometers (see e.g., de Moraes Frasson et al., 2011). However, disdrometers are designed to measure rainwater drops, which have optical properties that differ greatly from those of metal. This goes beyond simply obstructing the light beam and

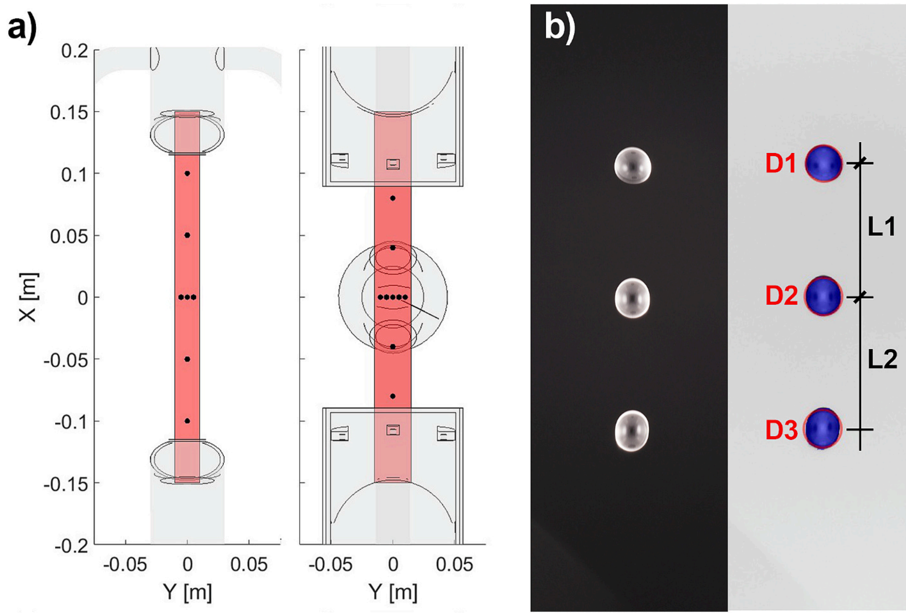

Fig. 2. a) Schematics showing the crossing positions investigated over the instrument's sensing area for the Thies LPM (left) and OTT Parsivel^2 (right) disdrometers. b) Example of the image obtained from the PVS and the automated post-processing of a generated 3 mm drop.

may result in an additional bias due to the methodology used for testing rather than to the instrument's performance. Scarce information is available in literature about this problem when calibrating disdrometers.

For this reason, an initial testing of both the Thies LPM and the OTT Parsivel^2 disdrometers was carried out by releasing calibrated steel spheres of various diameters, ranging from 1 mm to 5 mm in 0.5 mm increments, over the instrument's sensing area. The spheres were released individually using a 3D-printed dispenser with the PVS diffuser acting as a positional reference. This was done from a constant height of 37 cm, with the test repeated at least 30 times for each investigated position over the instrument's sensing area.

A total of seven positions were tested for the Thies LPM and nine for the OTT Parsivel^2, which has a larger beam. The investigated locations form a cross, with five positions parallel to the laser beam and five perpendicular to it (three in the case of the Thies LPM), sharing the central position. Fig. 2a shows a detailed scheme of the investigated crossing positions. The whole set of calibrated spheres was used at the centre of the laser beam, while a reduced set was used at the remaining positions.

When using water drops, the calibration of disdrometers is based on the comparison of the size and fall velocity of each drop as measured by the instrument with their reference values obtained from the PVS. Calibration tests were conducted for each instrument by generating six sets of water drops with a diameter between 0.6 mm and 5 mm. Drops were released from a fixed height of 1.2 m above the instrument's sensing area, ensuring that even the largest drops reached about 50% of their terminal velocity. Meanwhile, the centre of the PVS field of view is 32 cm above the instrument's sensing area. The same positions along the instrument's sensing area that were previously tested using metallic spheres were also tested using drops. No less than 30 drops were released for each position (and most often about 50 or more). As with the spheres, the full range of drop diameters was released at the centre of the instrument's sensing area, while only drops of 1, 3 and 5 mm in diameter were considered for the remaining positions.

During the laboratory tests, we noted that the measurements of the Thies LPM were affected by the flashes generated by the speedlights. Indeed, the instrument reports false drops when exposed to light flashes, with a reported drop diameter that is roughly proportional to the intensity of the light reaching the sensor. Shielding of the receiver was therefore implemented, using an opaque material to block light while permitting the passage of drops through small apertures positioned above and below the instrument laser beam. Furthermore, before each test the camera synchronization, focus and alignment between the DRH, the PVS and the instrument sensing area were rigorously verified, confirming the absence of any residual interference attributable to the speedlights. In the case of the OTT Parsivel^2, there were no instances of missing or false readings due to light flashes. Nevertheless, the OTT Parsivel^2 showed some false readings when large drops or large metallic spheres fall close to the receiving head. These false readings of ghost drops up to about 1 mm in diameter were found both in the raw data and in some of the PSVD matrix outputs.

2.3. *Image post processing*

The images obtained from the PVS (see an example in Fig. 2b on the left) provide the reference measurement for calibrating the disdrometers. Post-processing was automated using a machine vision algorithm, that identifies the drop's boundaries by analysing the high contrast created by the light from the diffuser on the drop contour against the black background. The code identifies the drop's contour and then calculates its cross-sectional area, the centre of mass, the maximum, minimum and equivolumetric diameters, under the hypothesis that the drop is radially symmetric with respect to the vertical axis during flight. Finally, the drop's velocity is determined by measuring the distance between consecutive images of the same drop and knowing the time interval between the flashes (2.5 milliseconds).

The data obtained from post-processing are visualised on the right-hand side of Fig. 2b. The drop area is shown in blue and the equivolumetric drop contour is shown in red (centred on the centre of mass). The traced distances L1 and L2 are also shown. The results of the algorithm were verified by comparing them with gravimetric measurements of several drops and by manually processing sample images. A detailed description of how this approach is traceable to the international standards is provided in Baire et al. (2022).

The results are presented below as the percentage relative bias between the measured and reference drop characteristics, or the quantities derived from them. The percentage relative bias for a generic variable X is calculated as follows:

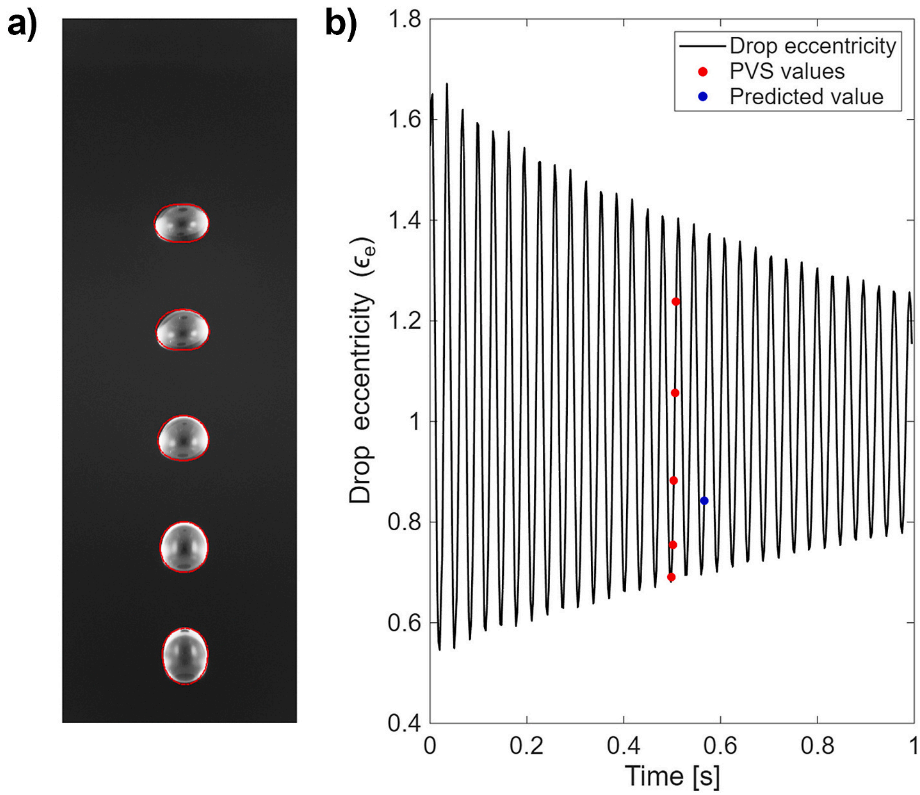

Fig. 3. Results of the analytical model (a) for the drop oscillation fitted to a 5 mm drop and superimposed (red circles) to the picture taken by the PVS. Evolution of drop eccentricity in time (b) for the same 5 mm drop: measured values from the PVS (red dots) and predicted value of the drop eccentricity when crossing the instrument's sensing area (blue dot).

$$e_X[\%] = \frac{X_{meas} - X_{ref}}{X_{ref}} \bullet 100 \quad (1)$$

where X_{meas} is the measured value of X provided by the disdrometer under test and X_{ref} is its reference value.

The reference size for metallic spheres is their nominal diameter. For water drops, instead, the reference size is the average equivolumetric diameter calculated from each individual photograph of the PVS. In the case of fall velocity measurements, the reference value is the average fall velocity calculated from each individual photograph of the PVS.

Disdrometers typically provide derived integral properties of precipitation like rainfall intensity (RI), kinetic energy flux (E) and radar reflectivity (Z), which are calculated from the measured PSVD matrix as shown in Eqs. (2), (3) and (4).

$$RI = \int_{D_{min}}^{D_{max}} N(D)V(D)\, v(D)\, dD \quad (2)$$

$$E = \int_{D_{min}}^{D_{max}} N(D)\ V(D)v(D)^3 dD \quad (3)$$

$$Z = \int_{D_{min}}^{D_{max}} N(D)D^6 dD \quad (4)$$

where *N(D)* is the number of drops per unit volume of air and unit drop size interval, *V(D)* is the drop volume assuming drops with spherical shape and *v(D)* is the drop fall velocity. Note that the coefficients containing numerical factors related to the conversion of the measurement units or properties independent on the drop size (such as the density of water) are omitted in the equations. These output variables are often used to compare disdrometer measurements with tipping-bucket or weighing rain gauge records (see, e.g., Johannsen et al., 2020b), with radar measurements (see, e.g., Adirosi et al., 2018) or evaluate soil erosion potential (see, e.g., Angulo-Martínez and Barros, 2015).

2.4. The impact of drop shape on calibration results

Images of larger drops (those above 2 mm in diameter) revealed clear oscillation of the drop shape during flight. This is primarily because larger drops only reach around 50% of their terminal velocity due to the limited release height, meaning they are far from equilibrium. Furthermore, the DRH itself inevitably induces some oscillations when the drop is detached from the nozzle. For this reason, specific tests were conducted to assess the effect that such oscillation – and therefore changes in the drop shape – may have on results. These tests involved slightly increasing the release height in increments of 10 mm, up to a maximum of 100 mm and releasing about 50 to 70 drops of 3 mm and 5 mm in diameter for each height. This was achieved by lowering the instrument under test using an adjustable mount, ensuring that the drops crossed the instrument's sensing area at different times during their oscillation cycle.

At the same time, an analytical model was used to simulate the oscillatory behaviour of drops falling through the PVS. This is based on Rayleigh's (1879) model, which describes the shape of an oscillating drop as a superposition of spherical harmonics. Although several authors used this approach, the work of Zhang et al. (2019) is the most relevant for this specific case. In that study, the model was used to validate the numerical simulation of a 3.72 mm diameter drop detached from a rigid support in conditions similar to those of the DRH. Although this model only considers axisymmetric modes and neglects nonlinear and aerodynamic effects, it provides a robust numerical framework for evaluating drop oscillation.

For the n^{th} mode of oscillation, the angular frequency (ω_n) is obtained as shown in Eq. (5), as derived by Miller and Scriven (1968) from the formulation of Lamb (1932).

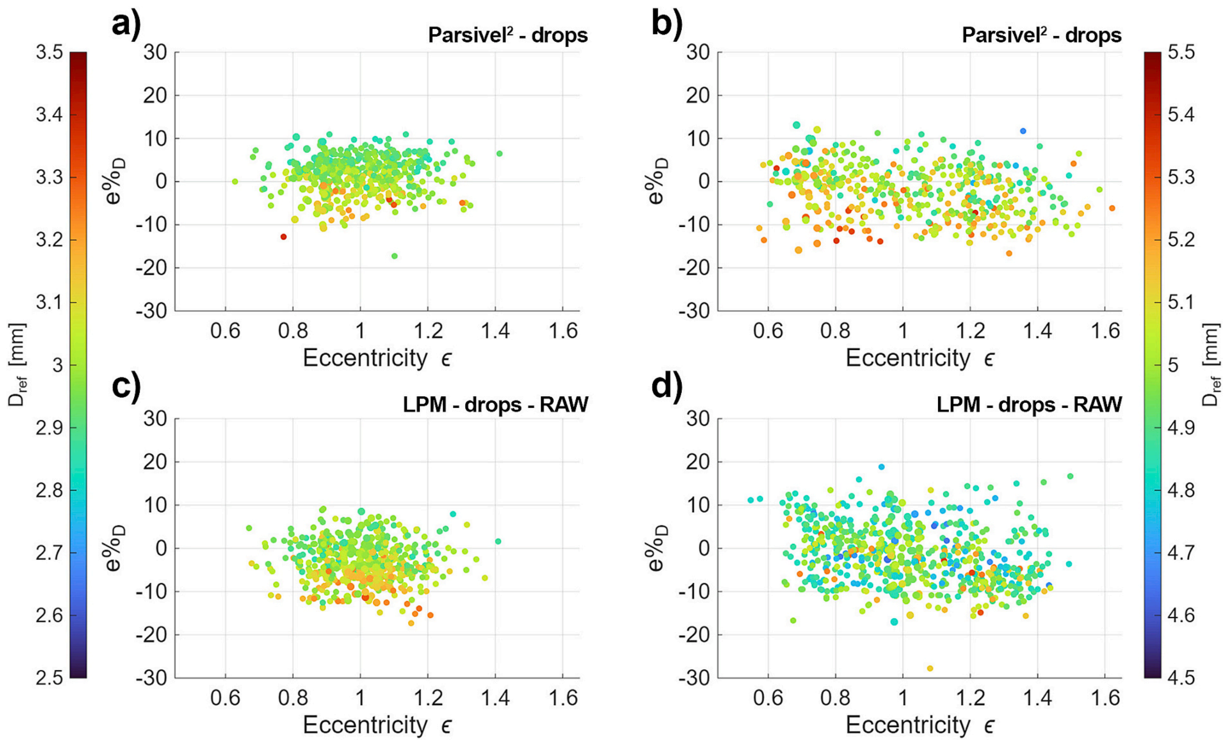

Fig. 4. Percentage relative bias in measuring drop diameter as a function of drop eccentricity (ε) when crossing the gauge sensing area (obtained from fitting the analytical model to the PVS images) for the OTT Parsivel^2 (a,b) and for the Thies LPM (c,d) and drops of 3 mm (a,c) and 5 mm (b,d). Dots are colour coded as a function of the reference drop equivolumetric diameter D_{ref} (obtained from the PVS).

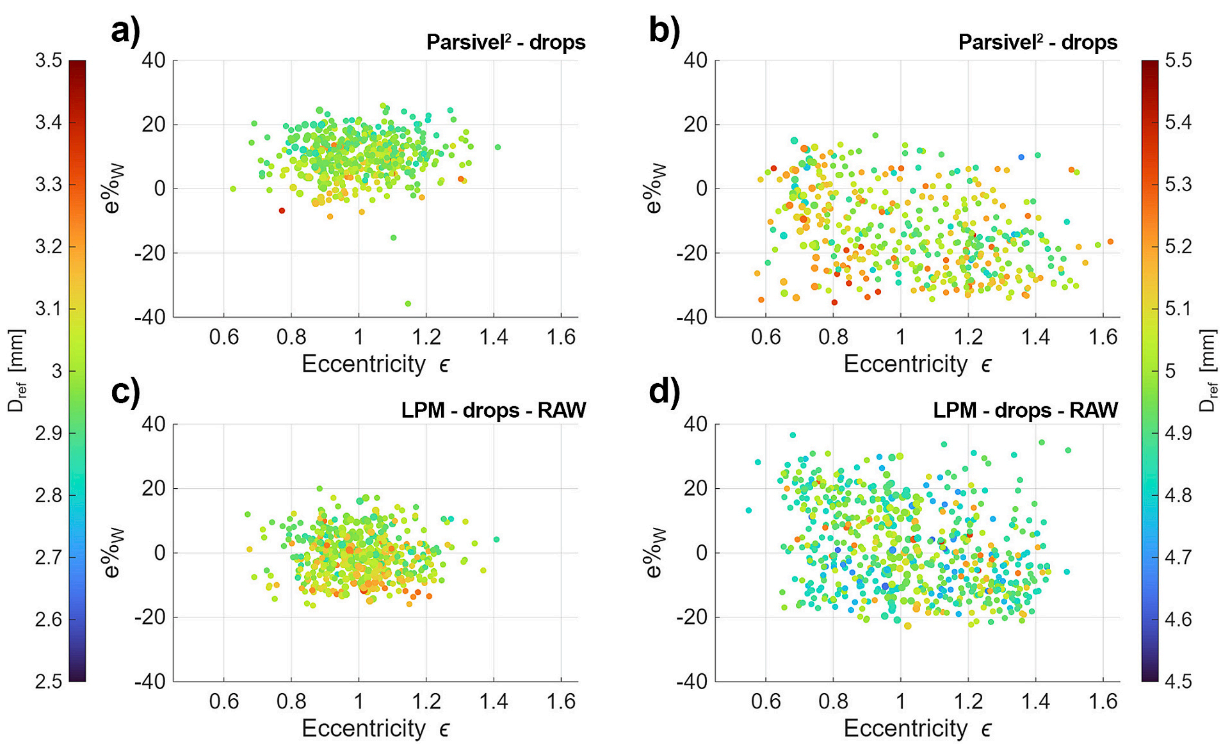

Fig. 5. Percentage relative bias in measuring drop fall velocity as a function of drop eccentricity (ε) when crossing the gauge sensing area (obtained from fitting the analytical model to the PVS images) for the OTT Parsivel^2 (a,b) and for the Thies LPM (c,d) and drops of 3 mm (a,c) and 5 mm (b,d). Dots are colour coded as a function of the reference drop equivolumetric diameter D_{ref} (obtained from the PVS).

$$\omega_n^2 = \frac{(n-1)n(n+1)(n+2)\sigma}{\left[(n+1)\rho_l + n\rho_g\right]R_D^3} - \frac{1}{\tau_n^2} \tag{5}$$

where R_D is the equivolumetric radius of the drop, σ is the surface tension, ρ_l is the density of water and ρ_g is the density of air. This formu-

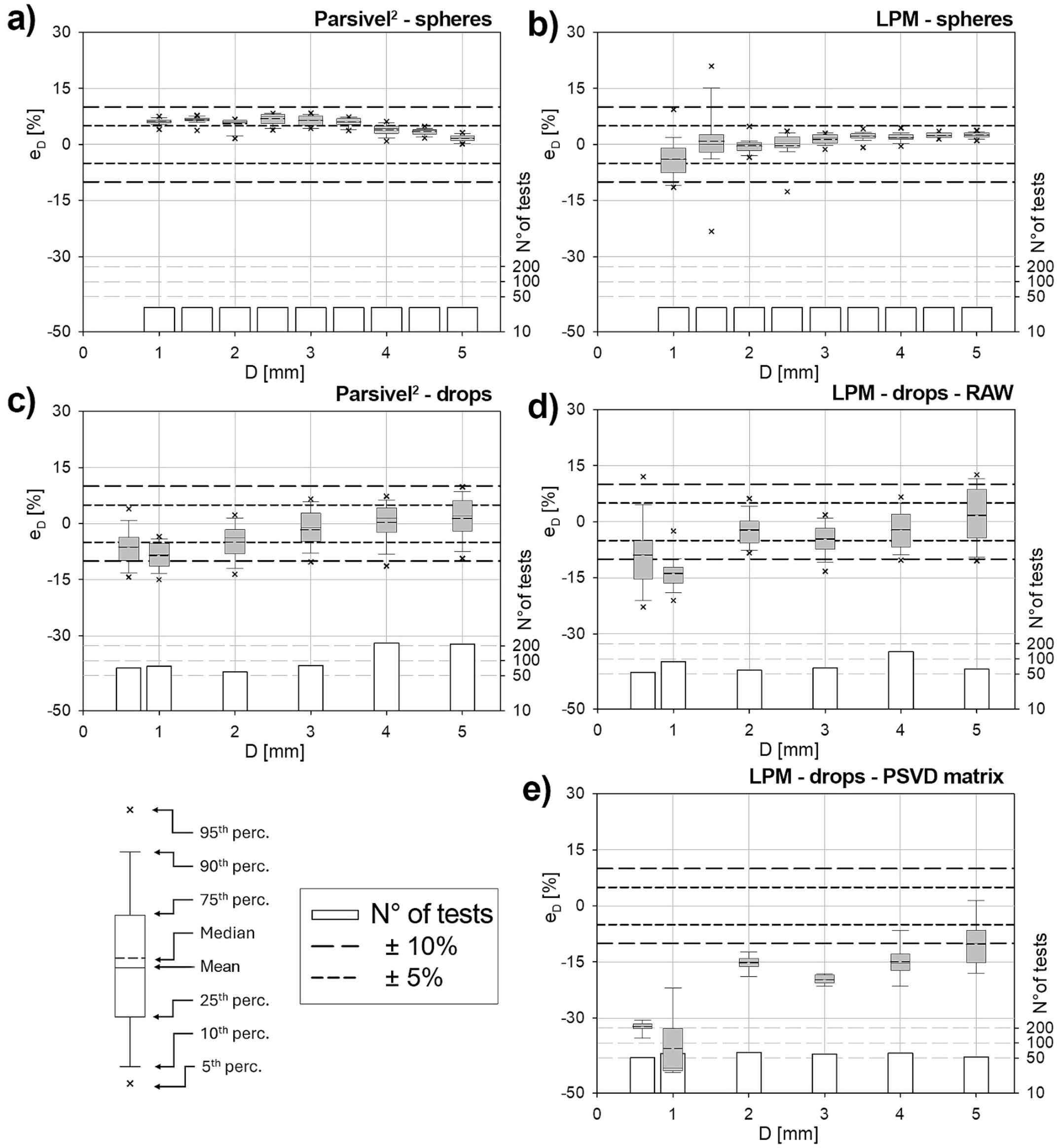

Fig. 6. Percentage relative bias in measuring drop size using metallic spheres (a,b) and water drops (c,d,e) for the OTT Parsivel² (a,c) and Thies LPM (b,d,e). The bias is computed using the raw measurements, except in panel (e), for which the results from the PSVD matrix are used for the Thies LPM. The spheres and water drops are released at the centre of the instrument's sensing area.

lation also accounts for the effect of water viscosity thanks to the term $\frac{1}{\tau_n{}^2}$, obtained from Eq. (6).

$$\tau_n = \frac{\rho_l \bullet R_D{}^2}{\nu_l (n-1)(2n+1)} \tag{6}$$

where ν_l is the kinematic viscosity of water. The drop shape is instead obtained as shown in Eq. (7).

$$R(\theta, t) = R_D \left\{ 1 + \sum_{n=0}^{\infty} A_n(t) \bullet P_n[\cos(\theta)] \right\} \tag{7}$$

$P_n[\cos(\theta)]$ is the Legendre polynomial of degree n and $A_n(t)$ is the corresponding Fourier-Legendre coefficient, as defined in Lamb (1932) and shown in Eq. (8).

$$A_n(t) = \alpha_n(t) \bullet \cos[\omega_n(t + \phi_n)] \tag{8}$$

where ϕ_n is the phase of the n-th mode of oscillation and $\alpha_n(t)$ is its amplitude, that decreases in time due to viscosity and is provided in Eq. (9).

$$\alpha_n(t) = \alpha_{n,0} \bullet \exp(-\beta_n \bullet t) \tag{9}$$

with $\alpha_{n,0}$ the initial amplitude and β_n the damping rate, also defined in the work of Lamb (1932) and shown in Eq. (10).

$$\beta_n = \frac{(n-1)(2n+1)\nu_l}{R_D{}^2} \tag{10}$$

The initial oscillation amplitude $\alpha_{n,0}$ and phase ϕ_n, depend on the shape and initial kinetic energy of the drop and are assumed to be a power law of the oscillation mode, in the form $\phi_n = c_{1\phi} \bullet n^{c_{2\phi}}$. The coefficients for both $\alpha_{n,0}$ and ϕ_n are obtained for each drop using a least square approach to fit its shape as captured by the PVS. The drop fall velocity is indeed measured and the flight time is known since it is a prerequisite to ensure the proper synchronization between the DRH and the PVS. This allows computing the shape of the oscillating drop when it crosses the laser beam. Examples of the resulting fit and the oscillating behaviour of a sample drop are shown in Fig. 3a and Fig. 3b, in terms of the drop eccentricity (ε). This is defined as the ratio between the vertical

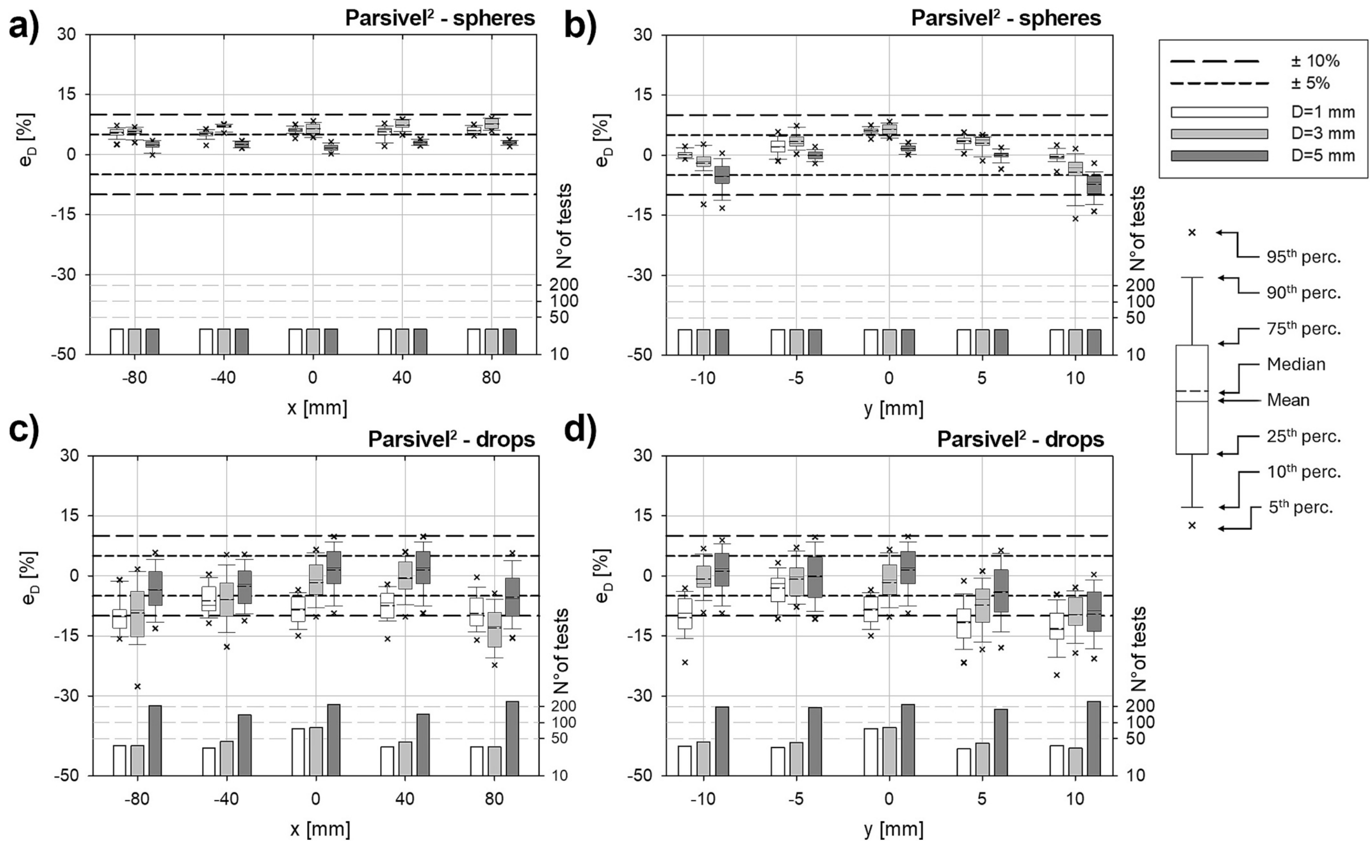

Fig. 7. Percentage relative bias in measuring drop size using metallic spheres (a, b) and water drops (c, d) using the OTT Parsivel^2. Test results for reference diameters of 1, 3 and 5 mm are presented for the five investigated positions along (a, c) and across (b, d) the laser beam.

and horizontal axis of the deformed drop. Values below unity indicate drops that cross the instrument's sensing area with a flattened shape that is close to the equilibrium shape of a drop falling at terminal velocity. Meanwhile, values equal to unity indicate spherical drops and values above unity indicate elongated drops with a shape that is opposite to the typical shape of a falling drop at terminal velocity.

Model fitting results are in good accordance with PVS observations, even if the model only considers linear effects for the oscillation and the hypothesis of radial symmetry around the vertical axis was made. The prediction of the drop eccentricity according to the fitted model (black continuous line), the eccentricity measured from the PVS images (red dots) and the predicted eccentricity of the drop when crossing the instrument's sensing area (blue dot) are presented in Fig. 3b.

Fig. 4 shows the scatterplots of the relative percentage bias in drop diameter measurements as a function of drop eccentricity when crossing the sensing area of the instrument. The plots are shown for drops with reference diameters of 3 mm (Fig. 4a and c) and 5 mm (Fig. 4b and d) for the two disdrometers investigated. For each test, between 500 and 700 drops were released from different heights above the centre of the instrument's sensing area. Each point is colour coded according to the reference drop equivolumetric diameter, obtained from the PVS. No significant trend in drop size measurement bias with respect to drop eccentricity is observed, even though the dispersion is quite significant. Only for drops of 5 mm in diameter and an eccentricity higher than 1.2 is a slight downward trend visible, especially for the Thies LPM.

An almost identical result is obtained when considering the relative percentage error in drop fall velocity, even though the results are more dispersed (see Fig. 5). Furthermore, a slightly more pronounced downward trend in relative percentage error in drop fall velocity is obtained for 5 mm drops. These results suggest that both instruments can account for variations in drop shape when calculating the equivolumetric diameter of the drop and its fall velocity. This can indeed be achieved by integrating or fitting the signal produced by the drop, rather than simply measuring the maximum obstruction of the laser beam.

However, the outcome of such integration may be significantly influenced by the sensor's sampling frequency, as well as the drop diameter and fall velocity. As pointed out in the work of Saha and Testik (2023), a non-negligible approximation may in fact be introduced by a limited or insufficient number of signal samples. This may explain the large variability of results and is consistent with the findings of Beczek et al. (2025). They observed an increase in the dispersion of the measurements as the release height increased, as well as a reduction in drop oscillation. The mean values showed limited change in the same work, even after a 4 m increase in release height, for both instruments. Based on the results shown in Fig. 4 and the above considerations, drops crossing the instrument's sensing area with an eccentricity above 1.2 were filtered out as they are generally not present in natural events.

3. Results and discussion

3.1. Bias in drop size and fall velocity measurements

Drop size is the most important measurand addressed by disdrometers, and accurate drop size measurements are fundamental to achieving a faithful reconstruction of the DSD. Fig. 6 shows the percentage relative bias in drop diameter measurements obtained for the two disdrometers investigated, based on laboratory calibration results and considering tests performed with both metallic spheres and water drops. For tests involving metallic spheres, the OTT Parsivel^2 (Fig. 6a) shows an overall overestimation of their diameter of more than 5%, which decreases as the size of the sphere increases beyond 4 mm. Dispersion is unexpectedly higher for medium-sized spheres (between 2.5 mm and 4 mm). Fig. 6b shows that the Thies LPM has limited bias and dispersion (within ±5%) when using metallic spheres for most

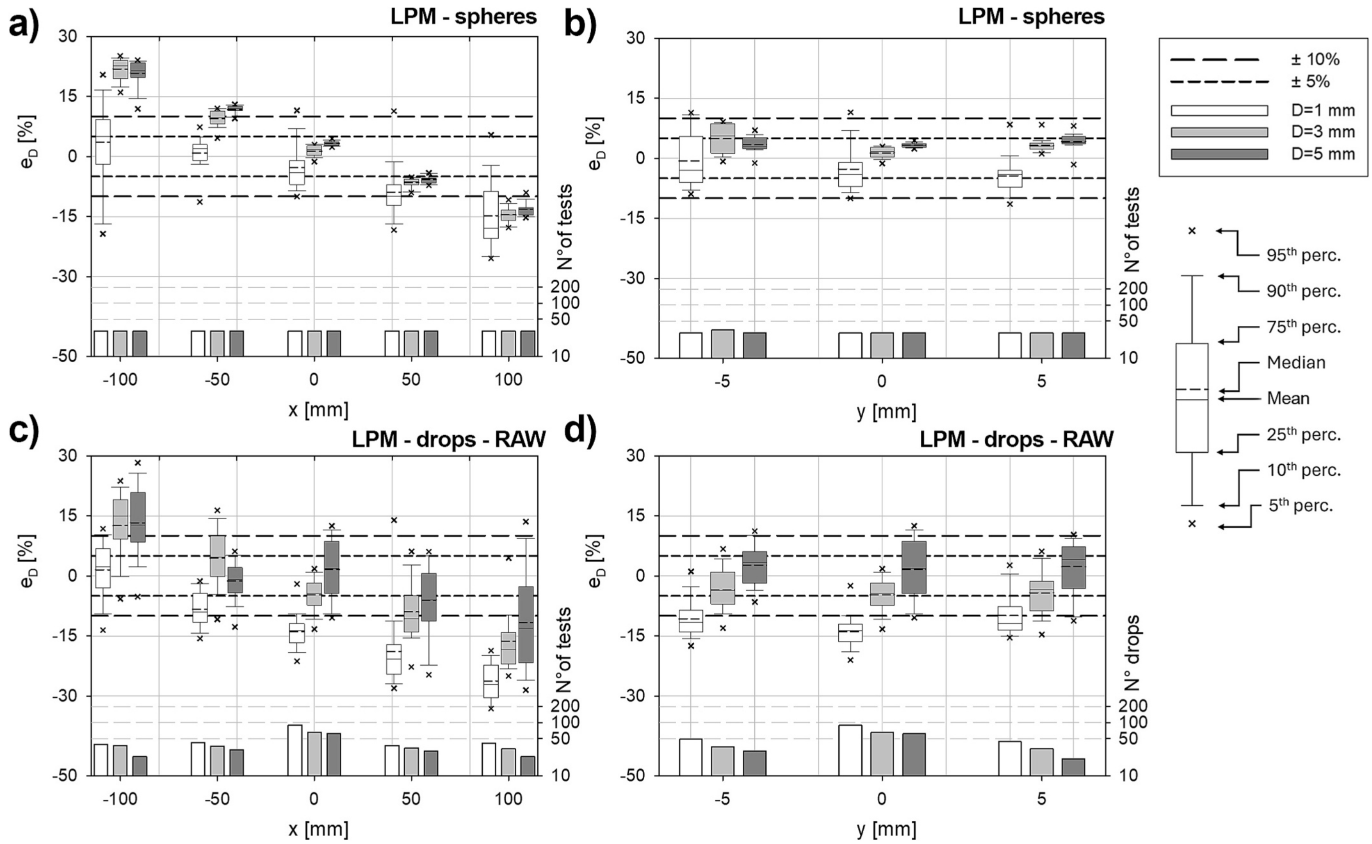

Fig. 8. Percentage relative bias in measuring drop size using metallic spheres (a,b) and water drops (c,d) for the Thies LPM. Test results for reference diameters of 1, 3 and 5 mm are presented for the five investigated positions along (a, c) and across (b, d) the laser beam.

diameters, except for 1 mm where underestimation is observed. This is opposite to the trend observed for the OTT Parsivel^2, since the absolute bias increases with the size of the sphere. While the mean bias is still low for 1.5 mm spheres, the dispersion is considerably larger below 2 mm.

The performance of both instruments deteriorates when water drops are used for calibration instead of metallic spheres. The dispersion of the results increases significantly, and the mean bias exhibits less consistent behaviour. However, the increased dispersion cannot be attributed to variability in the generated drop size around the nominal value, since the bias is calculated using the reference drop diameter obtained by capturing high-resolution images of individual drops in the PVS. Possible influencing factors include the different opacity of the medium and the increased fall velocity of the drops, which may introduce a larger sampling error (as discussed in the previous section).

When calibrating the OTT Parsivel^2 using water drops (see Fig. 6c), a less clear trend is observed, with a bias ranging from +5% to −10%. Drop diameter is generally underestimated, except for 4 mm and 5 mm drops, which are overestimated. The overall trend of the bias is the opposite of that observed with metallic spheres, while dispersion remains relatively constant throughout the diameter range. For the raw measurements of the Thies LPM (Fig. 6d), the bias shows slightly larger dispersion than for the OTT Parsivel^2, especially near the extremes of the tested diameters range. The overall trend of the bias is consistent with that observed for metallic spheres. However, dispersion seems to increase as the drop diameter increases, which is the opposite of what happens with spheres. This behaviour, whereby variability increases with drop size, is also evident in the work of Beczek et al. (2025), who only tested large drops with diameters ranging from 3.2 to 5.3 mm. Some underestimation is observed for water drops with diameters of 2 and 3 mm, while overestimation is observed for metallic spheres with the same nominal diameters.

The same overall trend is evident when using the PSVD matrix provided by the Thies LPM (Fig. 6e), albeit with significant underestimation. In this case, as only the number of drops in each bin was provided, tests were conducted with 5 or 10 drops released per minute. The bias was then computed using the mean of the reference values and the mean of the PSVD matrix, considering each drop to have a diameter or fall velocity equal to the mean bin value. For all nominal drop diameters, the percentage relative bias is approximately double, and in some cases almost triple, that obtained using the raw data. This significant difference cannot be explained by instrumental bias alone. Additional bias arises from the approximation that occurs when the drop diameter is assigned to one of the bins in the PSVD matrix. However, since the Thies LPM uses multiple bins to classify data, with particularly fine discretisation for smaller drops, the effect of this approximation is expected to be minimal. Instead, this discrepancy may be due to undisclosed internal post-processing of the instrument, which could result in the measured drop diameter being attributed to the incorrect bin.

Fig. 7 presents analogous results for additional crossing positions over the instrument's sensing area for the OTT Parsivel^2. In Fig. 7a,c) changing the crossing position along the laser beam has little effect on instrumental bias. However, the diameter of metallic spheres is overestimated by about 5% for all investigated positions, with larger spheres presenting a lower bias. Meanwhile, the drop diameter is mostly underestimated by about 5 to 10%, with the bias decreasing as the drop diameter increases. These results are consistent with those obtained at the centre of the laser beam. The same is true in terms of dispersion: results for metallic spheres show much lower dispersion than those for drops.

When considering the direction perpendicular to the laser beam (Fig. 7b,d), metallic spheres exhibit overestimation at the centre of the beam and underestimation near the edges. This trend remains visible in the case of drops despite a general underestimation is observed. Dispersion shows a similar trend, increasing from the centre of the beam

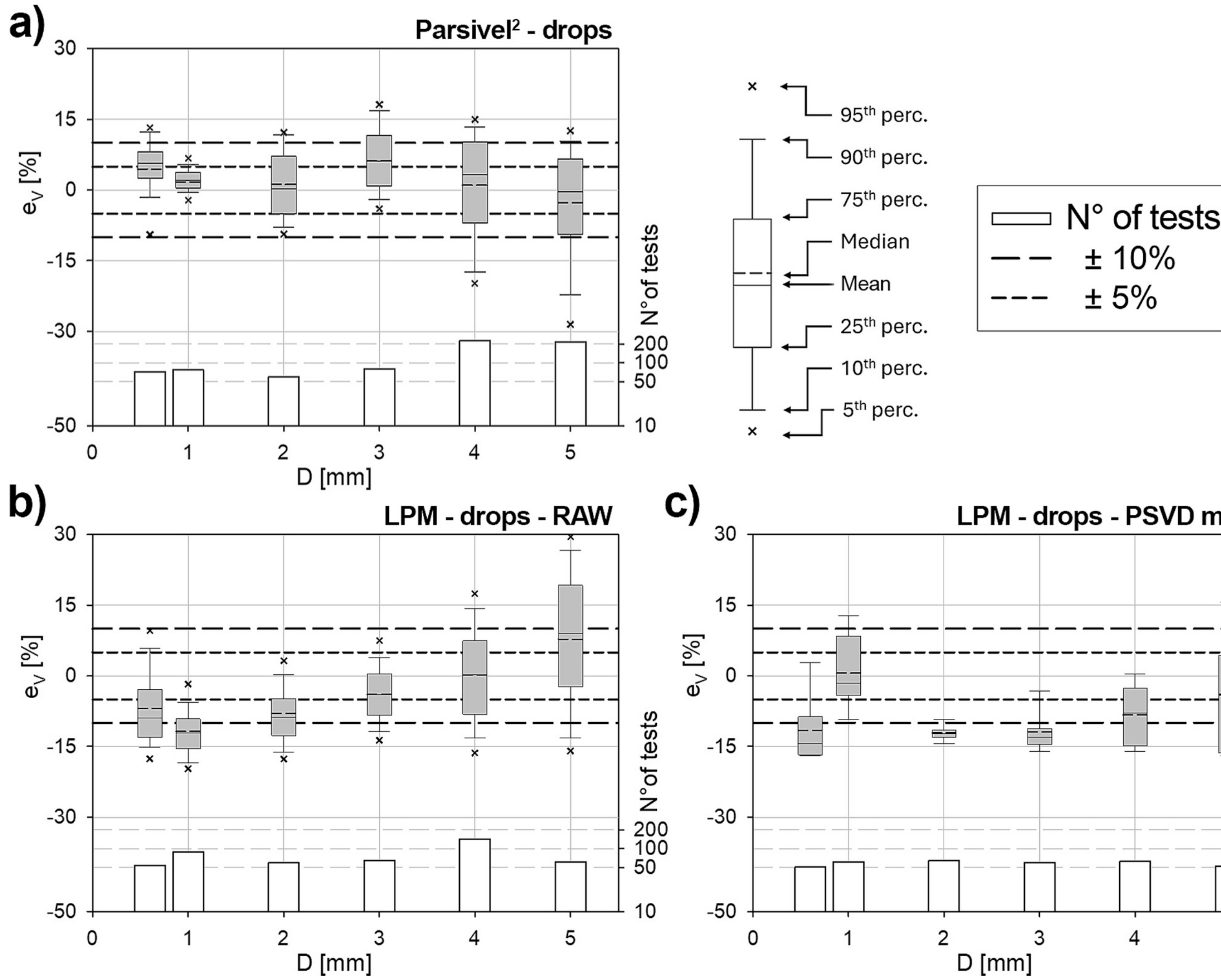

Fig. 9. Percentage relative bias in measuring drop fall velocity for the OTT Parsivel² (a) and the Thies LPM (b, c), as a function of the drop diameter. Test results were obtained using the raw measurements (a, b) and the PSVD matrix (c). All drops were released above the centre of the instrument's sensing area.

towards the edges.

Fig. 8 shows the results for different crossing positions of the laser beam for the Thies LPM. A clear trend is observed when moving along the laser beam (Fig. 8a,c). The diameter of spheres and drops released closer to the transmitter head is significantly overestimated, whereas those released closer to the receiver head are largely underestimated. Dispersion is also significantly greater away from the centre of the instrument's sensing area. Furthermore, a notable difference between metallic spheres and drops is evident, particularly for smaller diameters, with a significantly larger bias observed for water drops.

No clear trend is evident when considering the direction perpendicular to the instrument laser beam (Fig. 8b,d). However, one side of the instrument's sensing area shows greater dispersion, indicating that the laser beam may not be completely uniform. As in the previous case, comparing the results obtained from metallic spheres and water drops shows some differences, with larger overall bias being observed for the water drops.

Drop fall velocity is the second most important measurement taken by disdrometers. It is used to calculate both rainfall intensity and the kinetic energy of precipitation. No reference value is available for this measurand in the case of metallic spheres due to the release mechanism, so they were not considered in this analysis. Instead, the fall velocity of the released water drops is obtained from the PVS as the average of all the combinations that can be derived from multiple images of the same drops in each single photograph. Fig. 9 shows the percentage relative bias in fall velocity measurements for the two disdrometers investigated, based on laboratory calibration results for tests performed with water drops only.

The OTT Parsivel² (Fig. 9a) generally overestimates drop fall velocity by less than 5%. However, for 2 mm and 5 mm diameter drops, the mean bias is very close to zero, although dispersion is large. In contrast, the raw data for the Thies LPM (Fig. 9b) shows a general underestimation of drop fall velocity that decreases as the drop diameter increases. For both instruments, dispersion increases with an increase in drop diameter. This was also observed in the work of Beczek et al. (2025), albeit within a limited range of large drops. The results obtained from the PSVD matrix of the Thies LPM (Fig. 9c) are much closer to those obtained from the raw data than in the case of drop size measurements, although still worse. The only exception is for 1 mm diameter drops, which show overestimation instead of underestimation as when raw data are used. As with drop size measurements, this significant difference cannot simply be attributed to binning and may be due to the internal processing software.

Fig. 10 shows the percentage relative bias in measuring drop fall velocity obtained when releasing drops at different positions above the laser beam for both instruments. The OTT Parsivel² shows no trend in either direction (parallel or perpendicular to the laser beam), but significant underestimation of the fall velocity of larger drops is evident, alongside significant variability in the dispersion of the results (Fig. 10a, b). For the Thies LPM, the trend evident in drop size measurements is also apparent at various positions along the instrument laser beam (Fig. 10c). The fall velocity of drops crossing the laser beam close to the

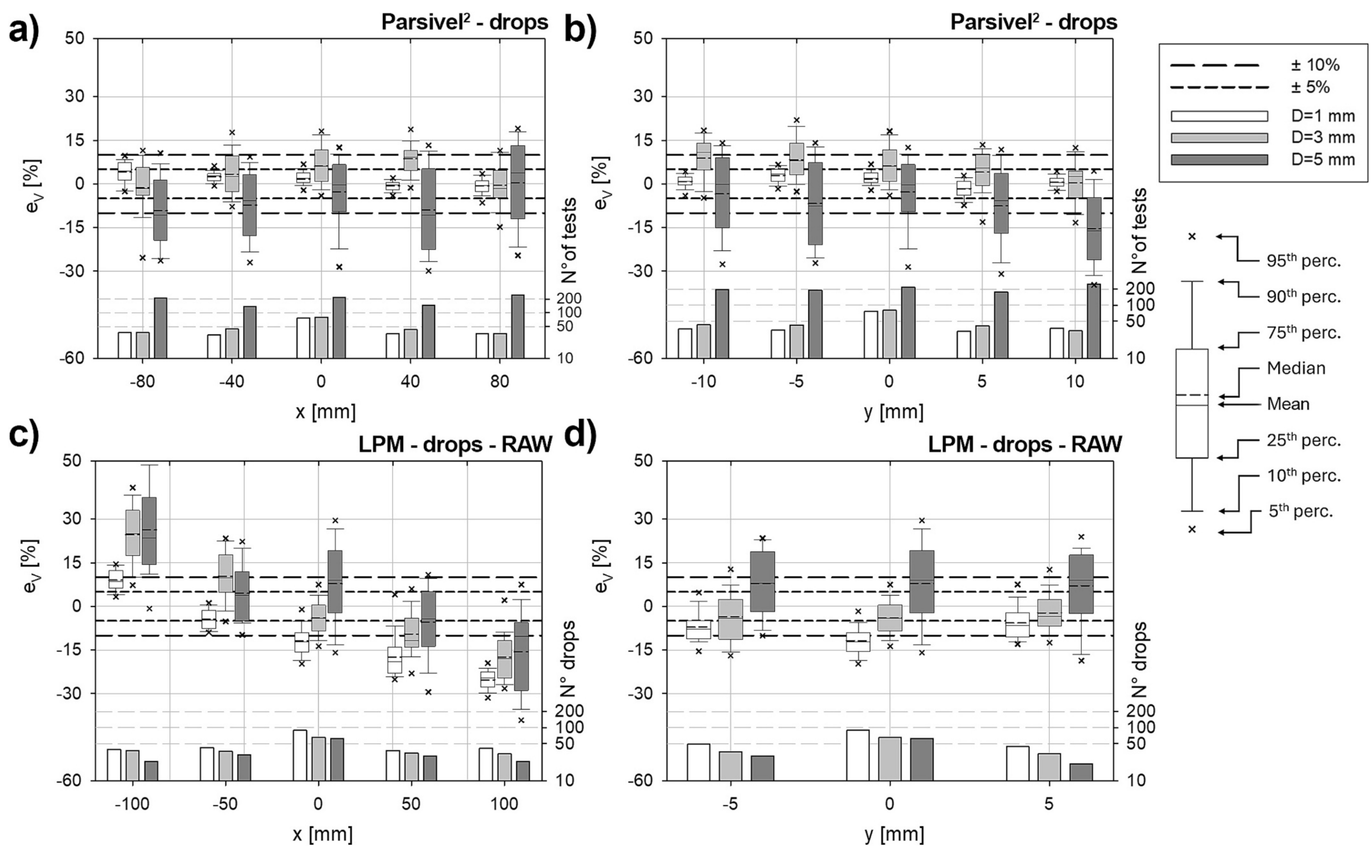

Fig. 10. Percentage relative bias in measuring drop fall velocity for the OTT Parsivel² (a,b) and the Thies LPM (c,d). Test results for reference diameters of 1, 3 and 5 mm are presented for the five investigated positions along (a, c) and across (b, d) the laser beam.

transmitter head is significantly overestimated, whereas the opposite is true for drops crossing close to the receiver head. There is no significant trend in terms of percentage relative bias and dispersion for positions across the laser beam (Fig. 10d).

3.2. Measurement of integral properties

We adopted a Monte Carlo approach to assess how measurement bias in drop size and fall velocity propagates into integral properties estimation using Eqs. (2), (3) and (4). This involves randomly selecting a set of drops (with the associated drop size and fall velocity information both measured by the PVS and the gauge), one for each diameter investigated, and assuming that this set is representative of a discretised DSD. Then, a mathematical form for the DSD is chosen. In this study, we selected the well-known exponential form of the Marshall–Palmer equation (Marshall and Palmer, 1948) with parameters that are linked to RI using the formulation proposed by (Cauteruccio and Lanza, 2020).

To derive the percentage relative bias, the measured integral properties can be computed by numerical integration and compared with the reference values, which are obtained by using the characteristics of the reference drops instead of the measured ones with the same DSD formulation. This process is repeated recursively by selecting drops at random from a uniform distribution. The ensemble mean and variance of the instrumental bias on the integral properties are then obtained. For this calculation, only the raw data telegram from the Thies LPM and the OTT Parsivel² were considered. Fig. 11 shows the resulting bias for the two investigated instruments as a function of the corresponding rainfall intensity (RI) value. We chose this representation because both E and Z are commonly expressed for operational purposes in relation to RI (that can be provided by traditional rain gauges), and the coefficients of the exponential form of N(D) are expressed in the literature as a function of RI.

Overall, the bias decreases as the intensity of the rainfall increases. This is to be expected, given that the bias for large drops is generally lower than for small ones. Both instruments tend to underestimate integral properties of precipitation, but the Thies LPM shows a larger overall bias. This is because the Thies LPM always underestimates both drop diameter and fall velocity, regardless of size. Meanwhile, the OTT Parsivel² shows both over- and underestimation of drop size and fall velocity, meaning the bias may be partially compensated for by integration. The OTT Parsivel² underestimates the RI by around 15% for lower values and around 10% for higher ones. The Thies LPM shows a similar trend, but with a much larger underestimation of around three times. The OTT Parsivel² underestimates the kinetic energy flux by about 5% up to an RI of 10 mm/h, while the bias is close to zero for a higher RI. The Thies LPM strongly underestimates E by up to 50% at the lowest RI.

When computing Z at low RI, small drops are prevalent in the DSD, resulting in underestimation by both instruments, while large drops are rare and do not significantly increase the calculated Z value. As RI increases, the Z bias decreases for both instruments because the contribution of large drops increases, and both instruments show less bias when measuring large diameters. The overestimation shown by the Parsivel² when measuring drops larger than 3 mm in diameter means the bias of Z reduces much faster with increasing RI than with the Thies LPM, reaching a mean bias close to zero at very high RI, as shown in Fig. 11.

4. Conclusions

The instrumental bias of optical disdrometers varies significantly depending on the size and fall velocity of the target hydrometeors. This was quantified in this work for liquid precipitation by calibrating two commonly used instruments in a laboratory and analysing their raw data

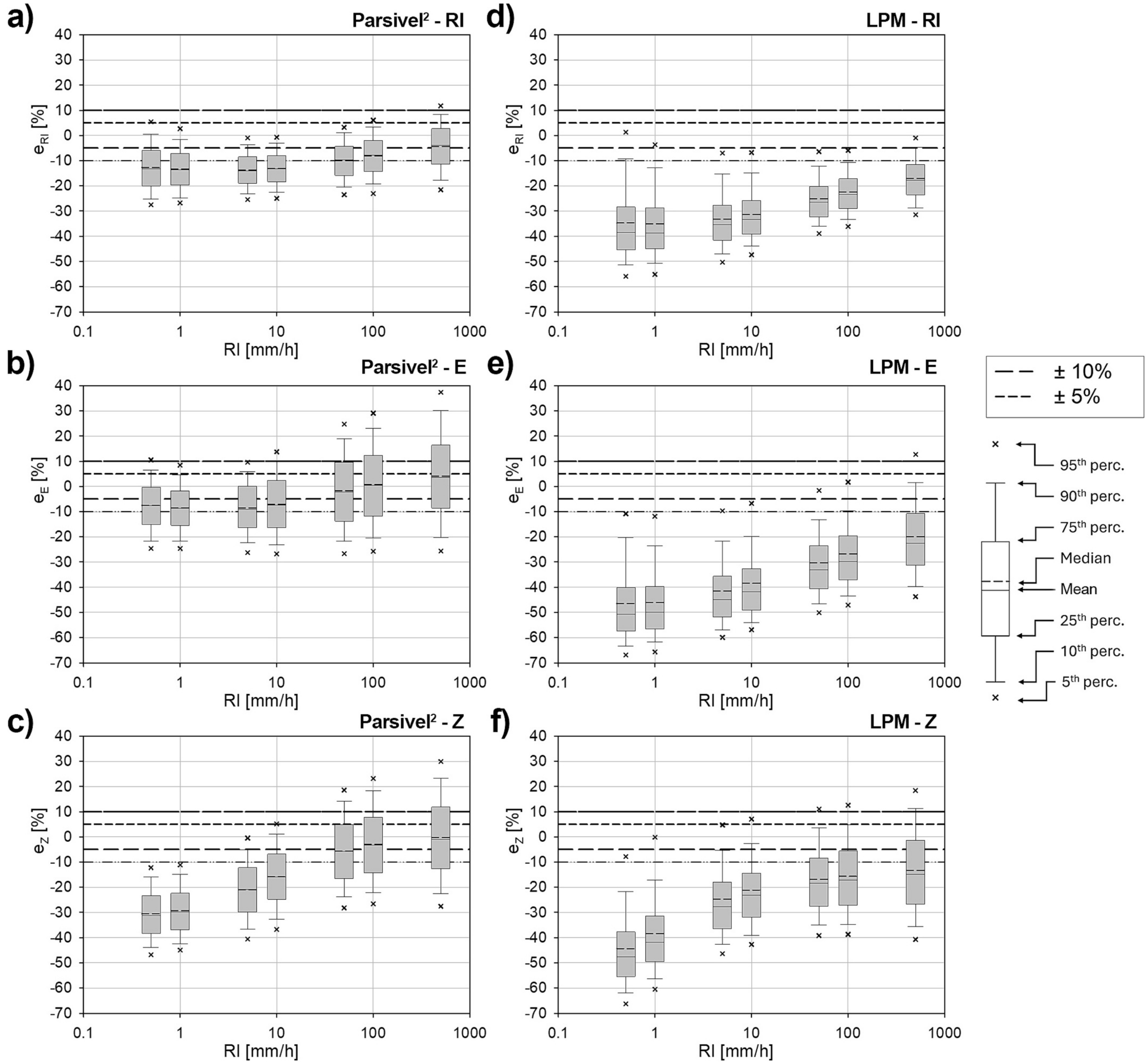

Fig. 11. Percentage relative bias in measuring precipitation integral properties for the OTT Parsivel^2 (a,b) and the Thies LPM (c,d), as a function of the corresponding rainfall intensity (RI) value.

output. A suitable raindrop generator was developed and used to provide a full-range characterisation of the instrument behaviour in terms of the percentage relative bias in measuring drop size and fall velocity, by releasing water drops of varying size with equivolumetric diameters between 0.6 and 5 mm from about 1.2 m above the instrument's sensing area. Metallic spheres were also used for calibration to demonstrate that significant differences in calibration results are obtained for both instruments when compared with the use of water drops. The accuracy and repeatability of measurements obtained using metallic spheres is not confirmed when water drops are used. This indicates that the calibration obtained using artificial particles is not appropriate for optical measurements of raindrop size and fall velocity.

The disdrometers investigated exhibit an approximately linear trend of the percentage relative bias when measuring both drop size and fall velocity as a function of the reference drop size. However, adjustment of field measurements may be challenging, given the large dispersion observed, especially for larger drops. Further research and technical development are needed to improve the accuracy of optical disdrometer measurements, particularly regarding the linearity of instrumental bias with drop size. Ideally, a reasonable trend would be established so that adjustment curves could be applied to raw measurements for practical use. To limit the dispersion observed in the laboratory tests, the repeatability of measurements should also be improved.

The results are much worse if we consider the output telegram providing the PSVD matrix, with even some totally unreported drops. This forced us to discard the PSVD output of the OTT Parsivel^2 from the calibration. This suggests that both instruments apply significant undisclosed filtering and/or post-processing. While some filtering may be necessary, the procedures and algorithms used by the instruments should be made available to end users for checking and calibration purposes.

False readings were also observed for both instruments. In the case of the OTT Parsivel^2 ghost drops of about 1 mm in diameter were observed when large drops (or spheres) fall close to the receiver head. Meanwhile, the Thies LPM reported false readings due to the flash produced by the speedlights in the PVS. These false readings may introduce an additional bias that is not quantified in this work, which could have a significant impact on field measurements.

The dispersion in drop size and velocity measurements is, on average, three times larger than the variability of the released drops as measured by the PVS. This dispersion increases as the drop diameter increases and is consistent with results reported in the literature (see, for example, Beczek et al., 2025). Specific tests to evaluate if drop oscillation could be responsible for this behaviour showed that the instruments are for the most part insensitive to drop oscillation. This is a positive feature since natural raindrops may oscillate during flight due to breakage or wind. This also suggest that reaching terminal velocity may not be a strict requirement when releasing large drops.

The work has obvious limitations, which do not invalidate the results obtained but require further research efforts. One limitation of this work is that only one instrument per model was tested, whereas differences in calibration results could be obtained within a set of instruments of the same model (evidence of this is already present in the literature). The physical properties of the water used for testing may also affect the results by changing how light is blocked by falling drops when they cross the laser beam. Tap water was used for the tests, but other types of water could be used, such as pure water or rainwater with different characteristics. These include the presence of solid particles (e.g., dust) or other substances that may be present in rainwater due to the wash-out of pollutants from the atmosphere. Further research is needed to determine how these factors affect the disdrometer ability to accurately measure drop size and fall velocity. Another limitation is the fall height of the water drops used in the tests due to the reduced size of the calibration device. The limited fall height means that the drops do not reach their terminal velocity, as would be expected in real-world conditions. Further work could involve increasing the fall height of the drops generated, in order to obtain a larger percentage of the velocity achieved in nature and check whether this limitation has any impact on the results.

The results highlight the necessity of a standardised procedure for calibrating non-catching precipitation measurement instruments, now available at European level (CEN, 2025). Such a procedure would enable manufacturers and end users to quantify the measurement bias associated with each instrument in a repeatable and traceable manner. It would also enable them to evaluate the impact of choosing any given model on their specific application and allow for meaningful comparisons of measurements taken with different instruments in different locations and under different environmental conditions.

CRediT authorship contribution statement

Enrico Chinchella: Writing – original draft, Visualization, Software, Methodology, Investigation, Formal analysis, Data curation. **Arianna Cauteruccio:** Writing – review & editing, Visualization, Validation, Methodology, Investigation, Formal analysis, Conceptualization. **Luca G. Lanza:** Writing – review & editing, Supervision, Resources, Methodology, Funding acquisition, Formal analysis, Conceptualization.

Declaration of competing interest

The authors declare that they have no known competing financial interests or personal relationships that could have appeared to influence the work reported in this paper.

Acknowledgments

The precision raindrop generator was developed as part of the EURAMET project 18NRM03, 'INCIPIT: Calibration and Accuracy of Non-Catching Instruments to Measure Liquid/Solid Atmospheric Precipitation'. INCIPIT received funding from the EMPIR programme, which is co-financed by the Participating States and the European Union's Horizon 2020 research and innovation programme. Laboratory testing of NCGs and evaluation of drop shape were carried out within the framework of the Italian National PRIN2022MYTKP4 project, 'Fostering innovation in precipitation measurements: from drop size to hydrological and climatic scales'. We would like to thank the Centro Tecnico per la Meteorologia (CTM) of the Italian Air Force and Yves-Alain Roulet from Météo Suisse for providing the disdrometers that were tested as part of this study.

Data availability

A link to the repository where data are available is provided.

Supplementary to "On the accuracy of optical disdrometer measurements" (Original data) (Mendeley Data)

References

Adirosi, E., Roberto, N., Montopoli, M., Gorgucci, E., Baldini, L., 2018. Influence of disdrometer type on weather radar algorithms from measured DSD: application to Italian climatology. Atmosphere 9 (9), 360. https://doi.org/10.3390/atmos9090360.

Adirosi, E., Montopoli, M., Bracci, A., Porcù, F., Capozzi, V., Annella, C., Baldini, L., 2021. Validation of GPM rainfall and drop size distribution products through disdrometers in Italy. Remote Sens. 13 (11), 2081. https://doi.org/10.3390/rs13112081.

Anagnostou, M.N., Anagnostou, E.N., Vivekanandan, J., Ogden, F.L., 2008. Comparison of two raindrop size distribution retrieval algorithms for X-band dual polarization observations. J. Hydrometeorol. 9 (3), 589–600. https://doi.org/10.1175/2007JHM904.1.

Angulo-Martínez, M., Barros, A.P., 2015. Measurement uncertainty in rainfall kinetic energy and intensity relationships for soil erosion studies: an evaluation using PARSIVEL disdrometers in the Southern Appalachian Mountains. Geomorphology 228, 28–40. https://doi.org/10.1016/j.geomorph.2014.07.036.

Aragon, L.G.B., Ibañez, M.P.A., Ordinario, R.C., Simpas, J.B.B., Cambaliza, M.O.L., Dado, J.M.B., Reid, E.A., 2024. Seasonal characteristics of raindrop size distribution and implication for radar rainfall retrievals in Metro Manila, Philippines. Atmos. Res. 311, 107669. https://doi.org/10.1016/j.atmosres.2024.107669.

Baire, Q., Dobre, M., Piette, A.S., Lanza, L., Cauteruccio, A., Chinchella, E., Garcia Izquierdo, C., 2022. Calibration uncertainty of non-catching precipitation gauges. Sensors 22 (17), 6413. https://doi.org/10.3390/s22176413.

Battaglia, A., Rustemeier, E., Tokay, A., Blahak, U., Simmer, C., 2010. PARSIVEL snow observations: a critical assessment. J. Atmos. Ocean. Technol. 27 (2), 333–344. https://doi.org/10.1175/2009JTECHA1332.1.

Beczek, M., Neumann, M., Mazur, R., Zumr, D., Dostal, T., Bieganowski, A., 2025. Challenges in measuring the size and velocity of large raindrops: a comparison of selected methods. J. Hydrol. https://doi.org/10.1016/j.jhydrol.2025.133932, 133932.

Bringi, V.N., Chandrasekar, V., Hubbert, J., Gorgucci, E., Randeu, W.L., Schoenhuber, M., 2003. Raindrop size distribution in different climatic regimes from disdrometer and dual-polarized radar analysis. J. Atmos. Sci. 60 (2), 354–365. https://doi.org/10.1175/1520-0469(2003)060%3C0354:RSDIDC%3E2.0.CO;2.

Burdanowitz, J., Klepp, C., Bakan, S., Buehler, S.A., 2018. Towards an along-track validation of HOAPS precipitation using OceanRAIN optical disdrometer data over the Atlantic Ocean. Q. J. R. Meteorol. Soc. 144, 235–254. https://doi.org/10.1002/qj.3248.

Campos, E., Zawadzki, I., 2000. Instrumental uncertainties in Z–R relations. J. Appl. Meteorol. 39 (7), 1088–1102. https://doi.org/10.1175/1520-0450(2000)039%3C1088:IUIZRR%3E2.0.CO;2.

Cauteruccio, A., Lanza, L.G., 2020. Parameterization of the collection efficiency of a cylindrical catching-type rain gauge based on rainfall intensity. Water 12 (12), 3431. https://doi.org/10.3390/w12123431.

CEN, 2025. EN 18097:2025 Metrological Requirements and Test Methods for Non-Catching Type Rain Gauges.

Chatterjee, C., Das, S., 2020. On the association between lightning and precipitation microphysics. J. Atmos. Sol. Terr. Phys. 207, 105350. https://doi.org/10.1016/j.jastp.2020.105350.

Chinchella, E., Cauteruccio, A., Lanza, L.G., 2024. Quantifying the wind-induced bias of rainfall measurements for the Thies CLIMA optical disdrometer. Water Resour. Res. 60 (10), e2024WR037366. https://doi.org/10.1029/2024WR037366.

Chinchella, E., Cauteruccio, A., Lanza, L.G., 2025. Impact of wind on rainfall measurements obtained from the OTT Parsivel^2 disdrometer. Sensors 25, 6440. https://doi.org/10.3390/s25206440.

Colli, M., Lanza, L.G., La Barbera, P., Chan, P.W., 2014. Measurement accuracy of weighing and tipping-bucket rainfall intensity gauges under dynamic laboratory testing. Atmos. Res. 144, 186–194. https://doi.org/10.1016/j.atmosres.2013.08.007.

Colli, M., Stagnaro, M., Caridi, A., Lanza, L.G., Randazzo, A., Pastorino, M., Caviglia, D. D., Delucchi, A., 2019. A field assessment of a rain estimation system based on earth-to-satellite microwave links. IEEE Trans. Geosci. Remote Sens. 57 (5), 2864–2875. https://doi.org/10.1109/TGRS.2018.2878338.

Conrick, R., Zagrodnik, J.P., Mass, C.F., 2020. Dual-polarization radar retrievals of coastal Pacific Northwest raindrop size distribution parameters using random forest regression. J. Atmos. Ocean. Technol. 37 (2), 229–242. https://doi.org/10.1175/JTECH-D-19-0107.1.

de Moraes Frasson, R.P., Da Cunha, L.K., Krajewski, W.F., 2011. Assessment of the Thies optical disdrometer performance. Atmos. Res. 101 (1–2), 237–255. https://doi.org/10.1016/j.atmosres.2011.02.014.

Disdromet, 2022. Disdrometer RD-80. In: Operating Instructions. Distrometer Ltd., Switzerland. https://distromet.com.

Fencl, M., Dohnal, M., Valtr, P., Grabner, M., Bareš, V., 2020. Atmospheric observations with E-band microwave links–challenges and opportunities. Atmos. Meas. Tech. 13 (12), 6559–6578. https://doi.org/10.5194/amt-13-6559-2020.

Gatidis, C., Schleiss, M., Unal, C., 2022. Sensitivity analysis of DSD retrievals from polarimetric radar in stratiform rain based on the μ–Λ relationship. Atmos. Meas. Tech. 15, 4951–4969. https://doi.org/10.5194/amt-15-4951-2022.

Giannetti, F., Lanza, L.G., 2023. Special issue "rain Sensors". Sensors 23 (15), 6934. https://doi.org/10.3390/s23156934.

Gires, A., Bruley, P., Ruas, A., Schertzer, D., Tchiguirinskaia, I., 2020. Disdrometer measurements under Sense-City rainfall simulator. Earth Syst. Sci. Data 12 (2), 835–845. https://doi.org/10.5194/essd-12-835-2020.

Gorgucci, E., Scarchilli, G., Chandrasekar, V., Bringi, V.N., 2001. Rainfall estimation from polarimetric radar measurements: composite algorithms immune to variability in raindrop shape–size relation. J. Atmos. Ocean. Technol. 18 (11), 1773–1786. https://doi.org/10.1175/1520-0426(2001)018%3C1773:REFPRM%3E2.0.CO;2.

Gunn, R., Kinzer, G.D., 1949. The terminal velocity of fall for water droplets in stagnant air. J. Atmos. Sci. 6 (4), 243–248. https://doi.org/10.1175/1520-0469(1949)006%3C0243:TTVOFF%3E2.0.CO;2.

Jadhao, V.G., Pandey, A., Mishra, S.K., 2023. Modeling of rain erosivity employing simulated rainfall and laser precipitation monitor. Model. Earth Syst. Environ. 9 (4), 4477–4492. https://doi.org/10.1007/s40808-023-01727-0.

Johannsen, L.L., Zambon, N., Strauss, P., Dostal, T., Neumann, M., Zumr, D., Klik, A., 2020a. Impact of disdrometer types on rainfall erosivity estimation. Water 12 (4), 963. https://doi.org/10.3390/w12040963.

Johannsen, L.L., Zambon, N., Strauss, P., Dostal, T., Neumann, M., Zumr, D., Cochrane, T.A., Blöschl, G., Klik, A., 2020b. Comparison of three types of laser optical disdrometers under natural rainfall conditions. Hydrol. Sci. J. 65 (4), 524–535. https://doi.org/10.1080/02626667.2019.1709641.

Joss, J., Waldvogel, A., 1967. Ein spektrograph für niederschlagstropfen mit automatischer auswertung. Pure Appl. Geophys. 68 (1), 240–246. https://doi.org/10.1007/BF00874898.

Kathiravelu, G., Lucke, T., Nichols, P., 2016. Rain drop measurement techniques: a review. Water 8 (1), 29. https://doi.org/10.3390/w8010029.

Kummerow, C., Simpson, J., Thiele, O., Barnes, W., Chang, A.T.C., Stocker, E., Nakamura, K., 2000. The status of the tropical rainfall measuring mission (TRMM) after two years in orbit. J. Appl. Meteorol. 39 (12), 1965–1982. https://doi.org/10.1175/1520-0450(2001)040%3C1965:TSOTTR%3E2.0.CO;2.

Lamb, H., 1932. Hydrodynamics, § 156. Univ. Press, Aufl., Cambridge, pp. 1879–1932, 427.

Lane, J.E., Kasparis, T., Metzger, P.T., Jones, W.L., 2014. In situ disdrometer calibration using multiple DSD moments. Acta Geophys. 62, 1450–1477. https://doi.org/10.2478/s11600-014-0237-2.

Lanza, L.G., Cauteruccio, A., 2022. Accuracy assessment and intercomparison of precipitation measurement instruments. In: Precipitation Science. Elsevier, pp. 3–35. https://doi.org/10.1016/B978-0-12-822973-6.00007-X.

Lanza, L.G., Vuerich, E., 2009. The WMO field intercomparison of rain intensity gauges. Atmos. Res. 94 (4), 534–543. https://doi.org/10.1016/j.atmosres.2009.06.012.

Lanza, L.G., Merlone, A., Cauteruccio, A., Chinchella, E., Stagnaro, M., Dobre, M., Parrondo, M., 2021. Calibration of non-catching precipitation measurement instruments: a review. Meteorol. Appl. 28 (3), e2002. https://doi.org/10.1002/met.2002.

Lee, J., Byun, J., Baik, J., Jun, C., Kim, H.J., 2023. Estimation of raindrop size distribution and rain rate with infrared surveillance camera in dark conditions. Atmos. Meas. Tech. 16 (3), 707–725. https://doi.org/10.5194/amt-16-707-2023.

Levia, D.F., Hudson, S.A., Llorens, P., Nanko, K., 2017. Throughfall drop size distributions: a review and prospectus for future research. Wiley Interdiscip. Rev.: Water 4 (4), e1225. https://doi.org/10.1002/wat2.1225.

Marshall, J.S., Palmer, W.M.K., 1948. The distribution of raindrops with size. J. Atmos. Sci. 5 (4), 165–166. https://doi.org/10.1175/1520-0469(1948)005%3C0165:TDORWS%3E2.0.CO;2.

Merlone, A., Musacchio, C., Coppa, G., Lanza, L.G., Cauteruccio, A., Chinchella, E., Roulet, Y.-A., Dobre, M., Baire, Q., Piette, A.-S., Nielsen, J., Kjeldsen, H., Østergaard, P., García Izquierdo, C., Parrondo, M., Kowal, A., 2022. The INCIPIT project: calibration and accuracy of non-catching instruments to measure liquid/solid atmospheric precipitation. In: WMO/CIMO Technical Conference on Meteorological and Environmental Instruments and Methods of Observation, Paris, 10–13 October 2022.

Miller, C.A., Scriven, L.E., 1968. The oscillations of a fluid droplet immersed in another fluid. J. Fluid Mech. 32 (3), 417–435. https://doi.org/10.1017/S0022112068000832.

Mocholí Belenguer, F., Martínez-Millana, A., Mocholí Salcedo, A., Milián Sánchez, V., Anaya, Josefa Palomo, M., 2020. Disdrometer performance optimization for use in urban settings based on the parameters that affect the measurements. Symmetry 12 (2), 303. https://doi.org/10.3390/sym12020303.

Nanko, K., Moskalski, S.M., Torres, R., 2016. Rainfall erosivity–intensity relationships for normal rainfall events and a tropical cyclone on the US southeast coast. J. Hydrol. 534, 440–450. https://doi.org/10.1016/j.jhydrol.2016.01.022.

OTT Hydromet GmbH, 2017. Operating Instructions Present Weather Sensor OTT Parsivel2. Kempten, Germany.

Park, S.G., Kim, H.L., Ham, Y.W., Jung, S.H., 2017. Comparative evaluation of the OTT PARSIVEL 2 using a collocated two-dimensional video disdrometer. J. Atmos. Ocean. Technol. 34 (9), 2059–2082. https://doi.org/10.1175/JTECH-D-16-0256.1.

Peinó, E., Bech, J., Polls, F., Udina, M., Petracca, M., Adirosi, E., Gonzalez, S., Boudevillain, B., 2024. Validation of GPM DPR Rainfall and drop size Distributions using Disdrometer Observations in the Western Mediterranean. Remote Sens. 16, 2594. https://doi.org/10.3390/rs16142594.

Petersen, W.A., Kirstetter, P.E., Wang, J., Wolff, D.B., Tokay, A., 2020. In: The GPM ground validation program. In: Satellite Precipitation Measurement, 2. Springer International Publishing, Cham, pp. 471–502. https://doi.org/10.1007/978-3-030-35798-6_2.

Pryor, S.C., Barthelmie, R.J., Cadence, J., Dellwik, E., Hasager, C.B., Kral, S.T., Veraart, M., 2022. Atmospheric drivers of wind turbine blade leading edge erosion: review and recommendations for future research. Energies 15 (22), 8553. https://doi.org/10.3390/en15228553.

Rayleigh, L., 1879. On the capillary phenomena of jets. Proc. R. Soc. Lond. 71–97. https://www.jstor.org/stable/113738.

Saha, R., Testik, F.Y., 2023. Assessment of OTT Parsivel^2 raindrop fall speed measurements. J. Atmos. Ocean. Technol. 40 (5), 557–573. https://doi.org/10.1175/JTECH-D-22-0091.1.

Schleiss, M., Smith, J., 2015. A method to estimate the 3D–time structure of the raindrop size distribution using radar and disdrometer data. J. Hydrometeorol. 16, 1222–1242. https://doi.org/10.1175/JHM-D-14-0182.1.

Sheppard, B.E., 1990. Measurement of raindrop size distributions using a small Doppler radar. J. Atmos. Ocean. Technol. 7 (2), 255–268. https://doi.org/10.1175/1520-0426(1990)007%3C0255:MORSDU%3E2.0.CO;2.

Špačková, A., Bareš, V., Fencl, M., Schleiss, M., Jaffrain, J., Berne, A., Rieckermann, J., 2021. A year of attenuation data from a commercial dual-polarized duplex microwave link with concurrent disdrometer, rain gauge, and weather observations. Earth Syst. Sci. Data 13 (8), 4219–4240. https://doi.org/10.5194/essd-13-4219-2021.

Tapiador, F.J., Navarro, A., Levizzani, V., García-Ortega, E., Huffman, G.J., Kidd, C., Turk, F.J., 2017. Global precipitation measurements for validating climate models. Atmos. Res. 197, 1–20. https://doi.org/10.1016/j.atmosres.2017.06.021.

Tapiador, F.J., Berne, A., Raupach, T., Navarro, A., Lee, G., Haddad, Z.S., 2018. Objective characterization of rain microphysics: validating a scheme suitable for weather and climate models. J. Hydrometeorol. 19 (6), 929–946. https://doi.org/10.1175/JHM-D-17-0154.1.

Tokay, A., Kruger, A., Krajewski, W.F., 2001. Comparison of drop size distribution measurements by impact and optical disdrometers. J. Appl. Meteorol. Climatol. 40, 2083–2097. https://doi.org/10.1175/1520-0450(2001)040<2083:CODSDM>2.0.CO;2.

Thies A., 2011. Instruction for Use. Adolf Thies GmbH and Co.

Tokay, A., D'Adderio, L.P., Wolff, D.B., Petersen, W.A., 2020. Development and evaluation of the raindrop size distribution parameters for the NASA Global Precipitation Measurement Mission ground validation program. J. Atmos. Ocean. Technol. 37 (1), 115–128. https://doi.org/10.1175/JTECH-D-18-0071.1.

Tuukka, P., 2015. Calibration of non-catching precipitation sensors at Vaisala. In: Presented at the ENV58 MeteoMet2 Workshop on Metrology for Essential climate Variables. University of Genova, Genoa, Italy, 11-12 March 2015.

Wu, Z., Zhang, Y., Zhang, L., Hao, X., Lei, H., Zheng, H., 2019. Validation of GPM precipitation products by comparison with ground-based Parsivel disdrometers over Jianghuai region. Water 11 (6), 1260. https://doi.org/10.3390/w11061260.

Yang, X., Jomaa, S., Rode, M., 2019. Sensitivity analysis of fully distributed parameterization reveals insights into heterogeneous catchment responses for water quality modeling. Water Resour. Res. 55 (12), 10935–10953. https://doi.org/10.1029/2019WR025575.

Zhang, B., Ling, Y., Tsai, P.H., Wang, A.B., Popinet, S., Zaleski, S., 2019. Short-term oscillation and falling dynamics for a water drop dripping in quiescent air. Phys. Rev. Fluids 4 (12), 123604. https://doi.org/10.1103/PhysRevFluids.4.123604.